Geology of the 5/22-1 (Errigal) exploration borehole, NE Rockall Basin, offshore western Ireland: the role of North Atlantic break-up magmatism on petroleum systems development

Christopher A-L. Jackson
Craig Magee
Carl Jacquemyn

Basins Research Group (BRG), Imperial College, Prince Consort Road, LONDON, SW7 2BP, England, UK

email: c.jackson@imperial.ac.uk

ABSTRACT

Large quantities of hydrocarbons reside in volcanically influenced sedimentary basins, many of which occur along continental margins. Despite the common assumption that magmatism negatively impacts petroleum system development, we actually have a poor understanding of its true role, largely due to a lack of studies utilising integrated subsurface datasets. In this paper we combine 3D seismic reflection, borehole, petrographic and paleothermometric data to document the geology of borehole 5/22-1, which drilled the Errigal prospect, NE Rockall Basin, offshore western Ireland. This borehole tested a large four-way dip closure (i.e. a forced fold) that formed to accommodate forcible emplacement of a Paleogene igneous sill-complex during North Atlantic continental breakup. The borehole was unsuccessful, with only very minor traces of dead hydrocarbons discovered in Upper Paleocene deep-water siltstones. Two water-wet turbidite sandstone-bearing intervals occur in the Upper Paleocene. The lower interval contains two *c*. 5 m thick, quartzose-feldspathic sandstones of good reservoir quality, and several thin (<4 m), very poor-quality volcaniclastic sandstones containing abundant pore-filling and pore throat-bridging clay minerals. In contrast, the upper interval is dominated by the very poor-quality volcaniclastic sandstones, derived from a volcanic terrain genetically related to the magmatism driving forced folding and trap formation; the poor reservoir quality in this interval reflects diagenetic degradation of the abundant volcanic grains. Paleothermometric data, although of modest quality and quantity, provide equivocal evidence for magmatism-related elevated temperatures in the Paleocene-to-Eocene succession, suggesting sill-induced contact metamorphism and fluid flow were not solely responsible for the poor quality of the contained reservoirs; petrographic analysis suggests the poor reservoir quality likely reflects the abundance of volcanic grains and related clays derived from the

igneous rock-dominated, sediment source area. The reason for failure of the Errigal, which is located only *c*. 42 km NNW of the Dooish gas discovery, is unclear, but we speculate the low bulk permeability of the heavily intruded Cretaceous mudstone succession impeded vertical migration of sub-Cretaceous sourced hydrocarbons into supra-Cretaceous reservoirs. Although the failure of Errigal casts doubt on the prospectivity of this play type in this particular part of the NE Rockall Basin, breakup-related magmatism clearly drove formation of a large structural closure, with data from 5/22-1 at least providing evidence for the local development of reservoir-quality, Upper Paleocene, deep-water reservoirs and thick, Eocene topseals. Post-Cretaceous deep-water stratigraphic traps on the flanks of intrusion-induced forced folds represent potential future exploration targets, in addition to more conventional, rotated fault-block traps containing Mesozoic reservoirs.

INTRODUCTION

Stretching and thinning of the lithosphere during continental breakup drives upwelling and decompression melting of asthenospheric mantle (e.g. Allen & Allen, 2013). Magma formed during continental breakup may stall during its ascent to the Earth's surface, intruding the crust in the form of igneous sills and dykes. Because continental stretching precedes breakup, igneous intrusions are particularly common in some of the world's most prolific hydrocarbon provinces (e.g. offshore circum-Atlantic, e.g. Smallwood and Maresh, 2002; Rohrmann, 2007; Thomson & Hutton, 2004; Archer et al., 2005; Magee et al., 2014; Schofield et al., 2017; NW Shelf of Australia, Rohrmann, 2015; Magee et al., 2013; 2017, Reeckman and Mebberson, 1988; McClay et al., 2013). Petroleum systems in these provinces can and are commonly assumed to be negatively impacted by breakup-related magmatism. For example, sill and dyke intrusion can cause: (i) physical compartmentalization of stratigraphy, leading to dissection of reservoirs, or separation of source and reservoir rocks by impermeable sills and dykes; (ii) initiation of hydrothermal systems, with the local flow of anomalously hot fluids driving diagenesis at shallow depths and causing a reduction in reservoir quality; and (iii) overmaturation of source rocks (e.g. Rohrmann, 2003; Schutter, 2003; Holford et al., 2013; Eide et al., 2017). However, the discovery and production of hydrocarbons from igneous rocks demonstrate breakup-related magmatism may positively impact petroleum system development by: (i) causing the formation of structural and stratigraphic traps due to forced folding; (ii) creating a network of interconnected, potentially high-permeability intrusions that may act as either reservoirs (e.g. Reeckmann and Mebberson, 1988; Smallwood and Maresh, 2002; Schutter, 2003; Rohrmann, 2007; Witte et al., 2012; Magee et al., 2013; Egbeni et al., 2014; Bischoff et al., 2017), or as conduits that allow hydrocarbons to migrate from source rocks to reservoir rocks (e.g. Rateau et al., 2013; Rodriguez Monreal et al., 2009); (iii) driving the development of reservoir in surrounding host rock (e.g. by dolomitization; see Jacquemyn et al., 2014); or (iv) forming low-permeability seals (e.g. Schutter, 2003; Rodriguez Monreal et al., 2009). Despite being ubiquitous along petroliferous continental margins, there are surprisingly few studies detailing the impact breakup-related magmatism can have on petroleum systems development (see Schutter, 2003 and Rohrmann, 2007 for general reviews). We therefore have a limited conceptual framework within which to risk prospects and devise development plans in volcanically influenced basins.

To help improve our understanding of how breakup-related magmatism impacts petroleum systems development along continental margins, we here provide a detailed 'post-mortem' of exploration borehole 5/22-1, which tested the Errigal prospect, NE Rockall Basin (PEL 6/97), offshore western Ireland (Fig. 1). This borehole was drilled by Enterprise Energy Island Ltd and partners in 2001, targeting a large (*c*. 70 km^2) dome (i.e. four-way dip closure) situated *c*. 42 km NNW of the Dooish discovery (12/2-1), which was drilled in 2003 and represents the first commercial hydrocarbon discovery in the NE Rockall Basin (Figs 1 and 2). Borehole 5/22-1 took 26 days to drill to a total depth of 4070 m, in water depths >1500 m. The primary and secondary objectives were Upper and Lower Paleocene deep-water sandstones, respectively, sealed by latest Paleocene and Eocene shales (Fig. 1C). The prognosed trap and reservoir are underlain by an extensive, breakup-related, igneous sill-complex primarily intruded into Cretaceous strata (Figs 2 and 3) (Magee et al., 2014). Oil was predicted to be the main hydrocarbon phase, sourced from Lower Jurassic (pre-rift) or Upper Jurassic (syn-rift) marine mudstone. The well reached Upper Cretaceous rocks (Figs 1C and 2) and, despite penetrating a sandstone-bearing Eocene and Paleocene sequence, was plugged and abandoned as a dry hole, with only very minor traces of hydrocarbons being recorded in the target interval.

Although the failure of Errigal seemingly cast doubt on the prospectivity of this play type in at least this particular part of the NE Rockall Basin, data acquired during drilling provide an excellent opportunity to assess the role breakup magmatism had on petroleum systems development in this and possibly other volcanically influenced basins. We begin by briefly summarizing the tectono-magmatic and petroleum systems framework of the NE Rockall Basin, before using 3D seismic reflection and borehole data to constrain the structural and magmatic context of Errigal. We place particular emphasis on the origin and timing of the trap, and how this relates to breakup magmatism. We then use a range of predominantly pre-2004, now-released data, generously provided by the Department of Communications, Energy and Natural Resources (Petroleum Affairs Division), Ireland to: (i) describe and interpret spatial and temporal changes in the thickness and quality of the main Paleocene reservoir target (e.g. via final well reports, petrographic analysis); and (ii) constrain the paleothermometric evolution via fluid inclusion microthermometry (FI), vitrinite reflectance (VR) and apatite fission track analysis (AFTA) data of the basin, with a view to how this might relate to the inferred magmatic events and the observed reservoir quality. In addition to improving our understanding of petroleum systems development along the deep-water margin of western Ireland, the results of our study can also help us better understand the challenges associated similar prospects identified in other volcanically influenced basins.

GEOLOGICAL SETTING AND PETROLEUM SYSTEM ELEMENTS

The Rockall Basin is located along the NE Atlantic continental margin (Fig. 1). It is one of several deepwater (i.e. water depth of up to 1800 m) rifts that formed during initial opening of the North Atlantic (e.g. Doré et al. 1999; Naylor & Shannon 2005; Hansen et al. 2009). The earliest phase of breakup related extension occurred in the Permo-Triassic (‘syn-rift I’ of Magee et al., 2014; Figs 1C and 2), with a second phase of extension occurring in the Late Jurassic (‘syn-rift II’ of Magee et al., 2014; Figs 1C and 2) (e.g. Doré et al. 1999; Naylor & Shannon 2005; Tyrell et al. 2010). Crustal extension and fault-driven subsidence instigated a relative rise in sea-level and basin deepening, resulting in the deposition of a marginal-to-deep marine syn-rift succession, which is capped by a seismically mappable Hauterivian horizon (KH; Fig. 2) (e.g. Doré et al. 1999; Tyrell et al. 2010). Upper Jurassic marine shales were deposited during this transgression.

Northwards propagation of North Atlantic seafloor spreading during the late Early Cretaceous (Aptian-to-Albian) led to NW-SE-oriented extension and a third phase of rifting in the Rockall Basin (Doré et al. 1999). A deep marine, mudstone-dominated succession was deposited during this period of Early Cretaceous stretching (‘syn-rift III’ of Magee et al., 2014; Figs 1C and 2) (Naylor & Shannon 2005). Early Cretaceous extension was superseded by Late Cretaceous-to-Paleogene post-rift thermal subsidence; during this time, the deposition of deep-marine mudstones was intermittently interrupted in the Paleocene and Eocene by deposition of deep-water sandstones derived from a volcanic terrain that formed during the preceding period of breakup-related magmatism (see also Naylor & Shannon 2005; Haughton et al. 2005).

Paleocene deep-water sandstones and Eocene claystones represented the prognosed reservoir and seal, respectively, for the Errigal prospect. Upper Jurassic marine shales, in addition to underlying Carboniferous coals, represent two of the key source rocks in the Rockall Basin. The discovery of the Dooish gas condensate accumulation (c. 69 MMBOE), which contains a Mesozoic (Triassic-to-Middle-Jurassic), marginal marine-to-shallow marine sandstone located in a normal fault-bound, Late Jurassic rift-related structural trap, demonstrates the presence of a working petroleum system within the NE Rockall Basin (Fig. 1C and 2).

BREAKUP RELATED MAGMATISM AND ASSOCIATED DEFORMATION

Late Cretaceous-to-Early Eocene, breakup-related magmatism is common along the NE Atlantic Margin, manifesting as flood basalt lava flows, sill-complexes and volcanic centers (North Atlantic Igneous Province; Fig. 1A). The products of this magmatism have been identified and described using seismic reflection and borehole data from the North Rockall (Thomson & Hutton, 2004; Archer et al. 2005) and Irish Rockall basins (Fernandes, 2011; Magee et al., 2014). Igneous intrusions, in particular sills, are particularly common in the NE Irish Rockall Basin, being expressed in seismic reflection data as very high amplitude, typically strata-discordant reflections (Fig. 2) (Magee et al., 2014). The presence of intrusive igneous material in the NE Rockall Basin is confirmed by well 12/2-1, which penetrates a *c*. 14 m thick dolerite sill in Upper Paleocene mudstones overlying the Dooish discovery (e.g. Figs 1C and 4).

An extensive network of large, interconnected, saucer-shaped and inclined sills, which individually are up to 12.4 km long and cross-cut 1.8 km of stratigraphy, are developed north of Dooish (Fig. 2) (Magee et al., 2014). These intrusions are most densely stacked directly beneath the dome drilled by 5/22-1 and are largely hosted within Upper Cretaceous mudstone, although a few extend upwards into the Paleocene succession (Fig. 5). Based on the fact that sills are most densely stacked below the dome apex, and the observation that the Paleocene to Lower Eocene succession onlaps onto and thins across the dome (Figs 2 and 5), Magee et al. (2014) argue the dome represents a 'forced fold' that formed to accommodate incremental emplacement of magma over a *ca*. 15 Myr period during the Paleocene to Eocene. Thus, in common with many other volcanically influenced continental margins, the main period of magmatism in the NE Rockall Basin was broadly coeval with the acme of Late Cretaceous-to-Early Eocene continental breakup (Fig. 1C).

DATASET

Our dataset comprises: (i) digital seismic reflection and borehole data, much of which was presented by Magee et al. (2014) in their study of the tectono-magmatic history of the NE Rockall Basin; and (ii) 'analogue' data derived from now-released reports detailing previously confidential analyses undertaken immediately after drilling of 5/22-1 (Errigal) in 2001 and 12/2-1 (Dooish) in 2003 (see Supplemental Items 1-6, which are available upon request from the Department of Communications, Climate Action & Environment (Petroleum Affairs Division), Ireland via https://www.dccae.gov.ie/en-ie/natural-resources/topics/Oil-Gas-Exploration-Production/data/Pages/Data.aspx).

Seismic reflection data

The seismic dataset comprises a zero-phase, time-migrated, 3D seismic reflection survey that covers 2400 km^2. Inline (N-S) and crossline (E-W) spacing are 12.5 m (Fig. 1B). These data are displayed with a normal polarity, whereby a downward increase and decrease in acoustic impedance corresponds to a positive (red) and negative (blue) reflection, respectively (Fig. 2). We mapped four horizons: (i) Top Hauterivian (KH) (intra-syn rift III); (ii) Top Cretaceous (K) (near base reservoir); (iii) Top Paleocene (P) (near top reservoir); and (iv) Top Lower Eocene (E) (intra-post rift). Where data quality allows, we locally define and map an additional seismic horizon that corresponds to the intra-Cenomanian (KC) and likely demarcates the boundary between syn-rift III and younger post-rift rocks (Fig. 2). Interval velocities of 2250 m s^{-1} (seabed to E), 3220 m s^{-1} (E to K), and 4000 m s^{-1} (below K) were also calculated from the well data. Given that the dominant seismic frequency is *c*. 25 Hz in the stratigraphic interval of interest, interval velocities of 3220–4000 m s^{-1} suggest that the vertical resolution of the seismic data ranges from *c*. 32–40 m for the host rock succession (see Magee et al., 2014).

Borehole data

We use data from two boreholes (5/22-1; Errigal, and 12/2-1; Dooish) to constrain the age and lithology of the seismically mapped stratigraphic units (Figs 2 and 5). Both boreholes contain a full suite of well-log data, including gamma-ray (GR), density (RHOB), and velocity (DT) logs. A final well report was available for 5/22-1 (Supplemental Item 1), whereas composite logs (Supplemental items 2 and 6) and cuttings data (see information provided in Supplemental items 1, 2 and 6) were available for 5/22-1 and 12/2-1.

Petrographic data

Thin section descriptions and SEM analyses are provided in Supplementary Item 1.

Paleothermometric data

Paleothermometric data are provided in the form of several reports documenting the methods and analyses undertaken by the operator company and contractors soon after completion of the 5/22-1 (Errigal) in 2001. The paleothermometric analysis presented here includes the results of fluid inclusion microthermometric (Supplementary Item 3), and vitrinite reflection (VR) and apatite fission track (AFTA) analysis (Supplementary Item 4).

PALEOCENE RESERVOIR DISTRIBUTION, QUALITY AND PROVENANCE

Boreholes 5/22-1 (Errigal) and 12/2-1 (Dooish) encountered Upper Paleocene and Eocene deep-water sandstones (Fig. 4; see also Supplementary items 1-3). We here describe and interpret the distribution and quality, and infer the possible provenance of the Upper Paleocene sandstones.

Errigal

Description. 5/22-1 penetrated two deep-water turbidite sandstone-bearing intervals (Upper Paleocene 1 and 2) in the primary, Upper Paleocene objective; no sandstones were developed in the secondary, Lower Paleocene objective (Fig. 4; see also Supplementary items 1 and 2).

The upper sandstone-bearing interval (3505-3619 m; labelled 'Pal. 1' in Fig. 4) is *c*. 114 m thick and contains 1-4 m thick beds of generally well-sorted, subangular-to-subrounded, very fine-to-locally medium-grained volcaniclastic sandstones that contain "mafic" and "FeMg grains" (Fig. 6A and B; see also Supplementary items 1 and 2). Petrophysical analysis of the upper interval, using a Vcl cut-off of 50% (i.e. Vcl >50% is non-net) and a 10% porosity cut-off for net-sand, indicates that the net sand content (1.4 m) and net-to-gross (N:G) (<1%) of the upper interval is very low (Supplementary Items 1 and 2; see also Fig. 4). Thin section (Fig. 6B) and SEM analysis (Supplementary Item 1) reveals that chlorite and chlorite smectite (46% of the bulk rock volume), smectite and zeolites (analcime; 18% of the bulk rock volume) are the main cement phases, filling pores and clogging pore throats. Pyrite, gypsum and small amounts of carbonate and authigenic feldspar are also observed, in addition to volcanic glass fragments and tuffaceous material. Authigenic quartz is lacking, reflecting the lack of primary detrital quartz or inhibition of quartz precipitation due to the presence of chlorites (Supplementary items 1 and 2). Despite locally having a relatively high porosity (21%), reservoir quality in the upper interval is rather poor, with porosity being dominated by intercrystalline and grain dissolution-related microporosity (Supplementary Item 1).

The lower sandstone-bearing interval (3619-3930 m; labelled 'Pal. 2' in Fig. 4) is *c*. 311 m thick and contains scattered, generally thinner (<4 m and more commonly 1-2 m thick), volcaniclastic sandstones, of similar composition to the upper interval (see also Supplementary items 1 and 2). However, towards its base, this interval contains two c. 5 m thick, quartzose-feldspathic sandstones (3916-3926 m; Fig. 4). These sandstones are fine-to-medium-grained and moderately sorted, with individual grains being subangular. Thin-section (Fig. 6C) and SEM (Supplementary Item 1) analysis indicate that the quartzose-feldspathic sandstones have distinctly different cement phases and porosity systems to the immediately overlying sandstones or those within Upper Paleocene 1. First, they lack pore-filling and pore throat-bridging chlorite, chlorite smectite and zeolite, instead containing relatively limited amounts of illite and kaolinite, in addition to some carbonate cements (Fig. 6C); volcanic glass fragments are also absent. Second, well-connected interparticle macroporosity, instead of poorly developed intercrystalline and grain dissolution-related microporosity, is present in these sandstones (cf. Figs 6B and C; see also Supplementary Item 1). Petrophysical analysis of the entire lower interval, using the same criteria as the upper interval, indicates that the net sand content (8.1 m) and net-to-gross (N:G) (c. 3%) is very low (see Fig. 4), although the porosity of the basal quartzose-feldspathic sandstones is generally quite good (up to 16%) (Supplementary Item 1).

Interpretation. The volcanic sandstones and quartzose-feldspathic sandstones described above are petrologically distinct (Fig. 6). We interpret that the clay-rich nature of the volcanic sandstones dominating the Upper Paleocene succession likely reflects diagenetic degradation of the abundant volcanic grains forming the bulk of the primary depositional unit (Primmer et al, 1997). The volcanic clast- and volcanic glass-rich nature of these sandstones suggests that they were sourced from an onshore volcanic terrain dominated by basaltic igneous rocks, most likely within the British and Irish Paleogene Igneous Province, elements of which lay to the north of the NE Rockall Basin (Fig. 1A). In contrast to the volcanic terrain-derived sandstones, the quartzose-feldspathic composition of the sandstones at the base of Paleocene 2 is more consistent with derivation from a meta-sedimentary source area. We can interpret these compositional differences in one of two ways: (i) the sandstones were sourced from different locations; i.e. the majority of the sandstones were derived from a regionally extensive, volcanic source area, whereas the basal, quartzose-feldspathic sandstones were derived from a more local, meta-sedimentary source area; or (ii) the amount of contemporary volcanism changed through time; i.e. the basal, quartzose-feldspathic sandstones were deposited prior to emplacement of the widespread volcanic terrain that now dominates the northern basin margin, whereas most sandstones was deposited during later, and after widespread volcanism.

Dooish

Description. Because the Triassic and Jurassic, rather than Paleocene succession was the target of the well 12/2-1, only a completion log is available for the latter (Supplementary Item 5). These data indicate that the >500 m thick Upper Paleocene succession is mudstone-dominated; however, in its lower *c*. 150 m, it contains several 1.5-12 m thick sandstone beds in an overall silty, relatively low N:G interval (*c*. 20%) (Fig. 4; see also Supplementary Item 5). Texturally, these sandstones are fine-to-coarse-grained, angular to subrounded, and very well-sorted; compositionally they are composed of quartz, volcanic lithics and volcanic glass (Supplementary Item 5), similar to volcanic sandstone described in 5/22-1. In the upper part of the Upper Paleocene succession, a few 1-3 m thick beds of medium-to-coarse-grained, very well-sorted, subangular-to-subrounded sandstones occur (Fig. 4; see also Supplementary Item 5). These sandstones are compositionally very different to those encountered lower in the succession, being quartz-rich and lacking volcanic lithics or volcanic glass, similar to quartzose-feldspathic beds at the base of 5/22-1.

Interpretation. The Upper Paleocene succession encountered in 12/2-1 is markedly different to that in 5/22-1; i.e. quartzose sandstones occur near its base in 5/22-1 but near its top in 12/2-1, whereas volcaniclastic sandstones occur near its top in 5/22-1 but near its base in 12/2-1 (Fig. 4). The reason for this variability is unclear, although it might point to temporal and spatial changes in the provenance of the Paleocene deep-water sandstones, with time-equivalent sands being sourced from either a meta-sedimentary or a volcanic source area (see discussion above). However, due to a lack of biostratigraphic data we are unable to directly correlate Upper Paleocene sandstones between 5/22-1 and 12/2-1, and because the sandstones are relatively thin (<5 m) we are unable to directly map them in seismic reflection data. Nonetheless, seismic data clearly indicate that the Paleocene interval thins across the Errigal forced fold (see Magee et al., 2014), suggesting the structure grew during and may thus have influenced reservoir deposition (Smallwood & Maresh, 2002; Egbeni et al., 2014).

THERMAL HISTORY

Only traces of hydrocarbons are reported in 5/22-1, with the main Upper Paleocene sandstone-bearing intervals being water-wet (Supplementary items 1 and 6). However, dead oil was noted in intervening siltstones, which, along with the relatively nearby Dooish discovery, clearly indicates the presence of a working petroleum system in the NE Rockall Basin. As a corollary, these observations imply that source rocks are present in the basin, and that the thermal history of the basin led to maturation of these source rocks (see below). Given the basins tectono-stratigraphic development, its thermal history likely reflects: (i) regional (i.e. basin-scale) heating due to rifting; (ii) regional cooling due to post-rift shortening and uplift; and (iii) local heating driven by the emplacement of igneous intrusions, some of which extend upwards into the reservoir-bearing Paleocene succession (Fig. 2). It is likely that the former drove source rock maturation of Carboniferous coals for Dooish, which, although overlain by a single, 15 m thick intrusion, does not appear spatially related to a very large intrusion complex, unlike Errigal (Fig. 2). However, a key question is whether the latter (i.e. local intrusion-induced heating) was responsible for the poor reservoir quality observed within the Upper Paleocene succession in Errigal. More specifically, did contact metamorphism and/or intrusion-induced fluid circulation result in the degradation of volcanic grain assemblages, the clogging of pore space, blocking of pore throats and therefore the overall poor reservoir quality? To try and answer this question we examine fluid inclusion microthermometry (FI), vitrinite reflectance (VR) and apatite fission track analysis (AFTA) data obtained from sidewall core samples from the reservoir-bearing, Upper Paleocene succession (Supplementary items 3 and 4, which are synthesized in Figs 7-9). Taken together, data from these analyses could, at least conceptually, help determine the timing and magnitude of elevated palaeotemperatures that had been experienced by the reservoir. In this regard, we are particularly interested in whether emplacement of Paleocene-to-Early Eocene sills in Upper Cretaceous mudstones (Fig. 2), which was broadly coeval with but continued until after reservoir deposition, left a FI and/or VR or AFTA 'signal' in the reservoir-bearing, supra-sill succession.

Fluid Inclusion Microthermometry and fluorescence petrography

Microthermometry and fluorescence petrography was performed on fluid inclusions by the operator on samples from 12 sidewall cores taken from the Paleocene succession (Fig. 7; see also Supplementary Item 3). The aims of these analyses were two-fold: (i) to determine if chlorite-related cements in the upper sandstones were hydrothermal in origin or the product of low-temperature diagenesis; and (ii) to investigate if fluid inclusions contained any evidence for hydrocarbon migration into and subsequently out of the mapped structural closure.

Results. Primary aqueous fluid inclusions were found in analcime cement and authigenic quartz. The majority (91%; 31 of 34) of analcime-hosted primary inclusions were monophase, indicating formation below 60°C. However, some two-phase inclusions (9%, 3 of 34) are present that exhibit homogenization temperatures of 108°C to 119°C. (Fig. 7). Homogenisation temperatures recorded in primary inclusions of quartz overgrowths in the lowermost sandstones (3916 and 3925 m) range from 66°C to 82°C. Salinity of all primary inclusions is brackish (1.1-2.3% NaCl eq.) to low (0.1-0.5% NaCl eq.) for analcime and authigenic quartz, respectively.

Interpretation. Given that the present bottom hole temperature is 76°C, and based on the assumption that the rocks are, at present, at their maximum burial depth, most homogenization temperatures indicate trapping and/or resetting at temperatures consistent with their present burial depth. Some elevated homogenization temperatures suggest local resetting during a transient episode of elevated temperatures, likely related to a very brief period of localised hot fluid flow (see Supplementary items 3 and 4). This interpretation is supported by the observation that the majority of samples show no evidence for these locally elevated temperatures, and that generally low salinity indicates a fresh water influence in the diagenetic fluids. In an exclusively marine sequence, this fresh water component is either expulsed from non-marine sequences or the result of hydrous phases undergoing diagenesis. Chloritization or illitization of smectite lead to total loss of sodium and would thus increase formation water salinity (McKinley et al, 2003). Therefore, input from an external fresh water source is more likely to cause the observed salinity reduction.

One healed microfracture in a quartz grain contained petroleum- and associated water-bearing fluid inclusions (Supplementary Item 3). Precipitation and trapping occurred at higher temperatures (120-125°C) from a more saline (3.4% NaCl eq.) fluid than the observed analcime and authigenic quartz. Given the microfracture is present within a detrital grain, and that it contains evidence for a greatly different, more specifically warmer thermal history than other primary inclusions, we interpret that the microfracture contains inclusions trapping water transported with its host grain (i.e. the fluid was not trapped *in situ* but was rather 'inherited' from the grain source area; it does not therefore record the burial-related history of the sedimentary succession penetrated by 5/22-1).

Vitrinite Reflectance (VR)

Results. Vitrinite Reflectance was analysed for 26 cutting samples. Confidence levels for individual determinations is moderate to low, but no significant difference exist between the most and least reliable results. Despite confidence levels and scatter around the overall trend, comparison to AFTA results suggests a reliable VR assessment of maturity levels (Supplementary item 4). Reflectance values vary from 0.27% to 0.48%, corresponding to temperatures of <50C to 80°C (Fig. 8). Temperatures values increase, possibly non-linearly, with depth. The maturity of all samples, except for second shallowest sample at 0.27%, are higher than the calculated default thermal history (Supplementary item 4), determined by combining samples' burial history with present-day thermal gradient of 26.5°C/km.

Interpretation. VR maturity indicates that the sampled units have experienced hotter temperatures than their present-day temperatures. This temperature differential is on average 20°C higher. Due to scatter of the data, the non-linear trend of temperatures cannot be considered with confidence and could be confirmed or rejected by further detailed analyses. Non-linear temperature trend could indicate localized heating effect as a result of hot fluid movement or intrusive bodies.

Apatite Fission Track Analysis (AFTA)

Results. AFTA was performed on seven cutting samples (Supplementary item 4). In general, the high apatite yields and results are deemed to be of very high quality, providing reliable constraints on thermal history. Results are shown in Fig. 9. Apatites from all samples contain a large proportion of fission tracks formed prior to deposition. This will impact thermal history interpretation. For one of the samples, collected between 3575 and 3800 m, the mean length is 1.4 μm shorter than predicted, and cannot be explained as being inherited from the sediment source. Therefore this short mean length must represent the effects of higher temperatures after deposition. Lack of significant age reduction suggests heating was only moderate. In five out of 7 samples, fission track length is ~1.4-2 μm shorter than what is expected from default thermal history. This can be explained by either inherited signal from the sediment source terrain, or by the effect of elevated paleotemperatures after deposition or a combination of both. Maximum paleotemperatures would be between 15°C and 45°C above the present temperatures. For one sample only two track lengths were measured, and cannot be used to assess its thermal history.

Interpretation. Data from AFTA and VR give very consistent results. One AFTA sample unequivocally indicates it has cooled from temperatures around 80-100°C, prior to 10Ma. Overall the combination of AFTA and VR analyses suggest the onset of cooling of the studied samples from paleotemperatures 15-30°C above the present-day temperature sometime between 40 and 10Ma (conservative estimate).

DISCUSSION

Forced folds as hydrocarbon traps

The trap targeted by 5/22-1 is a forced fold, formed due to forcible emplacement of magma within an igneous sill-complex (Magee et al., 2014). Although this borehole was unsuccessful, similar structures have been targeted in other volcanically influenced basins, with varying degrees of success. For example, in 1983, exploration well Perindi-1, which is located in the NW Canning Basin, offshore NW Australia targeted one of several, relatively small (3-16 km^2 in areal extent; vertical closures of up to 120 m) forced folds developed above a suite of Permian saucer-shaped sills (Reeckmann and Mebberson, 1984). Although the well penetrated thick (i.e. several hundred meters), high-quality (>25% porosity) reservoirs, capped by a thick (50-90 m), the borehole was dry. However, the presence of oil shows indicates a working petroleum system, suggesting hydrocarbons migrated into and out of the structure. Reeckmann and Mebberson (1984) speculate Perindi-1 failed due to breaching of the seal by and loss of hydrocarbons along numerous normal faults developed at the dome crest. Because they are spatially restricted to the dome crest and because they die-out downwards, we infer that these faults formed due to outer-arc stretching of the fold during sill emplacement (cf. Hansen and

Cartwright, 2006; Magee et al., 2013; Magee et al., 2017). Sill emplacement may, therefore, drive growth of relatively large and therefore attractive forced fold-related traps, although a key risk is seal breaching by outer-arc stretching-related normal faults.

The Wichian Buri oil field, Phetchabun Basin, Thailand is an excellent example of a hydrocarbon accumulation associated with the emplacement of igneous rocks. In this location, emplacement of a dolerite laccolith caused forced folding of a lacustrine-fluvial clastic succession and formation of a large trap (Schutter, 2003 and references therein). Emplacement of a 'parasitic' intrusion, that was sourced from and which overlies the lower, main laccolith, forms the top seal to the accumulation. Hydrocarbons also occur within the intrusions themselves, presumably within emplacement-related fractures, with estimated recoverable reserves thought to be *c*. 30 MMbbl (Schutter, 2003). Wichian Buri is also notable in that emplacement of the laccolith is thought to be responsible for local maturation of otherwise immature source rocks. A similar situation arises in the Altiplanicie del Payún area of the Neuquen Basin, Argentina where otherwise immature source rock sections are intruded by a series of Tertiary laccoliths that are up to 600 m thick. The intruded clastic and carbonate rocks, in addition to the fractured igneous intrusions themselves, contain commercial oil accumulations (20–33°API) (Rodriguez Monreal et al., 2009). These examples highlight that sill emplacement and forced folding can generate viable hydrocarbon traps (Schmeidal et al., 2017).

In addition, it should be noted that uplift generated to accommodate the emplacement of an entire sill-complex can result in the amalgamation of forced folds, producing broad four-way dip closures that have greater amplitudes than individual forced folds developed above single intrusions (Magee et al., 2014). For example, whilst 5/22-1 targeted a *c*. 70 km^2 four-way dip closure (i.e. a forced fold), the structure forms part of a much broader area of uplift, termed a 'compound fold', which covers *c*. 224 km^2 and has a maximum amplitude of *c*. 385 m (Magee et al., 2014).

Why did Errigal fail?

No direct geochemical assessment of potential source rock intervals was undertaken in 5/22-1 and no significant oil shows were discovered, although traces were reported at 3420 m (Lower Eocene), 3690 m (Upper Paleocene) and 3900 m (Lower Paleocene) (Supplementary Item 6). However, based on a combination of spore fluorescence colors established during VR analysis, and despite the majority of the post-Cretaceous mudstones being determined to be no more than early mature (<0.6% Ro), extrapolation of this trend suggests Lower Paleocene and older strata may be just entering the oil window. Headspace and cuttings gas data provide only weak evidence for migrated hydrocarbons in the deeper, Cretaceous-to-Paleocene succession, in the form of thermogenic, relatively dry gas (Supplementary Item 6). In summary, high-quality source rocks are likely absent in the rather shallowly buried, largely post-Cretaceous succession, although there is some evidence that mature gas- and potentially oil-generating source rocks are present in the rift basin underlying Errigal. As such, it is not yet clear if 5/22-1 failed due to lack of source rock.

Although volcaniclastic deep-water sandstones are of generally poor-quality throughout the mudstone-dominated Upper Paleocene succession, thin intervals of good-quality reservoir occur (Fig. 4). As such, we do not consider that Errigal failed due to lack of reservoir. Despite seismic data presenting evidence for the direct, albeit only local juxtaposition of igneous sills and Upper Paleocene reservoirs, paleothermometric and mineralogical data, more specifically the smectite rather than illite-dominated nature of the preserved clays, do not present conclusive, evidence for widespread elevated paleotemperatures coeval with intrusion emplacement. Despite being based on different sample spacing within different parts of the Paleocene, paleothermometric data all suggest that, at some point in the past and to varying degrees, this succession experienced temperatures higher than encountered at present. This suggests that Paleocene-to-Early Eocene sill emplacement in Upper Cretaceous mudstones, predominantly below but locally at the same stratigraphic level as the reservoir intervals, did not trigger the initiation of a hydrothermal system in the Paleocene succession, or at least a system that was of sufficient areal extent and/or magnitude (in terms of maximum temperature) to be detected by any of the analytical techniques on the available samples as outlined above. An alternative interpretation is that the sill-induced hydrothermal system was hydraulically isolated and thus failed to connect to all reservoir intervals; this may account for the very rare occurrence of samples with evidence for relatively high temperatures and low salinities (Fig. 7). The Late Eocene timing of some elevated paleotemperatures inferred from AFTA data could, at least conceivably, partly overlap with the absolute latest phase of sill emplacement (Magee et al., 2014). Our interpretation that sill emplacement did not lead to establishment of a major hydrothermal system means that magma emplacement similarly did not play a role in the degradation of reservoir quality in the Upper Paleocene sandstones. From this we can infer that the poor-quality reservoir encountered in the well 5/22-1 was instead provenance- and diagenesis-controlled, occurring as a direct result of the volcaniclastic-dominated nature of the primary sediment. Low-salinity inclusions suggest input of low salinity fluids, either of meteoric origin or potentially from metamorphic fluids (Yardley & Graham, 2002) related to sill intrusion.

As we discussed above, intrusion-induced forced folds can be deformed by normal faults (Hansen & Cartwright, 2006; Magee et al., 2013; 2017), which may facilitate vertical leakage of hydrocarbons from otherwise valid traps (Reeckmann & Mebberson, 1984). Our seismic data present limited evidence for the widespread development of seismic-scale normal faults across the Errigal dome (Fig. 2). This implies outer-arc stretching-induced normal faulting probably did not cause the Errigal borehole to fail. Our interpretation is supported by the observation that one tentative hydrocarbon show was detected within the Errigal structure, implying hydrocarbons did not migrate into and then out of the trap; this contrasts with the Perindi borehole, offshore NW Australia described above (Reeckmann & Mebberson, 1984).

The Errigal trap is underlain by and genetically related to a geometrically complex, areally extensive network of largely interconnected sills (Fig. 2). In addition to our 82 seismically resolved and mapped sills, it is likely that additional, sub-seismic sills, in addition to sub-vertical and thus poorly imaged dykes, are present. Although we cannot constrain the permeability of individual sills or the sill-complex as a whole, and despite recent evidence that intrusions may be permeable to at least gas if not oil, due to the presence of cooling-induced fractures, it is likely that the bulk permeability of the sub-reservoir sill-complex is relatively low, especially when also considering potential contact metamorphism within surrounding Cretaceous mudstone. We therefore suggest that hydrocarbons expelled from pre-Cretaceous source rocks, and which filled the Dooish accumulation only *c*. 42 km to the south, were unable to migrate into the Errigal trap due to the baffling effects of the heavily intruded Cretaceous succession. These hydrocarbons may then have been diverted southwards, up structural dip, towards the fault-block trap penetrated by 12/2-1 (Dooish) (Fig. 2).

How might breakup-related magmatism influence future prospectivity in the NE Irish Rockall Basin?

Breakup-related magmatism in the NE Rockall Basin appears to have positively and negatively impacted on petroleum system development in this frontier basin. For example, emplacement of the igneous sill-complex drove Late Paleocene-to-Eocene growth of a dome-shaped forced fold, which represents a large, attractive, four-way dip closure (Fig. 5A). However, the extensive, largely impermeable sill-complex (Fig. 2) may have impeded vertical migration of hydrocarbons from deeper, pre-Cretaceous source rocks into shallower Paleocene reservoirs intervals. Furthermore, poor-quality reservoir within the target Paleocene interval (Fig. 6A and B) reflects sandstone derivation from a breakup-related volcanic source terrain that was genetically related to the offshore sill-complex.

Although Errigal failed, data collected during drilling are very useful, indicating reservoir-quality deep-water sandstones were at least locally deposited in the region during the Late Paleocene and Eocene, and that the Upper Paleocene, reservoir-bearing succession is capped by a thick, post-Eocene seal (Figs 1C and 4). As such, we consider that the post-Cretaceous succession of the NE Rockall Basin remains prospective. For example, although the intrusion-induced structural trap failed, additional prospectivity may remain in stratigraphic traps on the forced fold limbs. Intrusion-induced forced folding can drive syn-depositional deformation of the seabed, causing deflection and controlling the routing of sediment gravity-currents (Smallwood and Maresh, 2002; Egbeni et al., 2014). Turbidites may thin and onlap towards, and thus be absent at, the fold crest, a stratigraphic architecture that provides the opportunity for the development of stratigraphic traps. Charging such traps remains challenging due to the presence of the underlying, largely impermeable sill-complex, which may act to divert ascending hydrocarbons away from overlying traps.

ACKNOWLEDGEMENTS

The Department of Communications, Energy and Natural Resources (Petroleum Affairs Division), Ireland, is thanked for providing seismic and well data.

REFERENCES

Archer, S.G., Bergman, S.C., Iliffe, J., Murphy, C.M. & Thornton, M. (2005) Palaeogene igneous rocks reveal new insights into the geodynamic evolution and petroleum potential of the Rockall Trough, NE Atlantic Margin: Basin Research, 17, 171-201.

Bischoff, A.P., Nicol, A. & Beggs, M. (2017) Stratigraphy of architectural elements in a buried volcanic system and implications for hydrocarbon exploration. Interpretation, 5, SK141-SK159.

Doré, A.G., Lundin, E.R., Jensen, L.N., Birkeland, Ø., Eliassen, P.E. & Fichler, C. (1999) Principal tectonic events in the evolution of the northwest European Atlantic margin: Petroleum Geology of Northwest Europe: Proceedings of the 5th Conference, 41-61.

Egbeni, S., McClay, K., Fu, J.J.K., & Bruce, D. (2014). Influence of igneous sills on Paleocene turbidite deposition in the Faroe–Shetland Basin: a case study in Flett and Muckle sub-basin and its implication for hydrocarbon exploration: Geological Society, London, Special Publications, 397, 33-57.

Eide, C.H., Schofield, N., Jerram, D.A., & Howell, J.A. (2017) Basin-scale architecture of deeply emplaced sill complexes: Jameson Land, East Greenland. Journal of the Geological Society of London, 174, 23-40.

Emeleus, C.H. & Bell, B.R. (2005) British Regional Geology: the Palaeogene volcanic districts of Scotland, 4th edn. British Geological Survey, Nottingham.

Fernandes, K. (2011) Irish sills of the North Atlantic Igneous Province: seismic imaging, observations and implications for climate change. Unpublished Ph.D Thesis. University of Dublin, Trinity College, Dublin.

Hansen, D.M. (2006) The morphology of intrusion-related vent structures and their implications for constraining the timing of intrusive events along the NE Atlantic margin: Journal of the Geological Society of London, 163, 789-800.

Hansen, D.M., & Cartwright, J. (2006) The three-dimensional geometry and growth of forced folds above saucer-shaped igneous sills: Journal of Structural Geology, 28, 1520-1535.

Hansen, J., Jerram, D.A., McCaffrey, K. & Passey, S.R. (2009) The onset of the North Atlantic Igneous Province in a rifting perspective: Geological Magazine, 146, 309-325.

Haughton, P., Praeg, D., Shannon, P., Harrington, G., Higgs, K., Amy, L., Tyrrell, S. & Morrissey. T. (2005) First results from shallow stratigraphic boreholes on the eastern flank of the Rockall Basin, offshore western Ireland: Geological Society, London, Petroleum Geology Conference series, 6, 1077-1094.

Holford, S.P., Schofield, N., Jackson, C.A-L., Magee, C., Green, P.F. & Duddy, I.R. (2013). Impacts of igneous intrusions on source reservoir potential in prospective sedimentary basins along the western Australian continental margin. Proceedings of the Western Australia Basin Symposium.

Jacquemyn, C., El Desouky, H., Hunt, D., Casini, G. & Swennen, R. (2014) Dolomitization of the Latemar platform: Fluid flow and dolomite evolution: Marine and Petroleum Geology, 55, 43-67.

Magee, C., Briggs, F. & Jackson C.A-L. (2013) Lithological controls on igneous intrusion-induced ground deformation: Journal of the Geological Society of London, 170, 853-856.

Magee, C, Jackson, CA-L. & Schofield, N. (2013) The influence of normal fault geometry on igneous sill emplacement and morphology: Geology, 41, 407-410.

Magee, C., Jackson, C.A-L. & Schofield, N. (2014) Diachronous sub-volcanic intrusion along deep-water margins: Insights from the Irish Rockall Basin: Basin Research, 26, 85-105.

Magee, C., Jackson, C.A-L., Hardman, J.P., & Reeve, M.T. (2017) Decoding sill emplacement and forced fold growth in the Exmouth Sub-basin, offshore northwest Australia: Implications for hydrocarbon exploration: Interpretation, 5, SK11-SK22.

McClay, K., Scarselli, N. & Jitmahantakul, S. (2013) Igneous intrusions in the Carnarvon Basin, NW Shelf, Australia: The sedimentary basins of Western Australia IV: Proceedings of the Petroleum Exploration Society of Australia Symposium, Petroleum Exploration Society of Australia, 1–20.

McKinley, J.M., Worden, R.H. & Ruffell, A.H. (2009) Smectite in Sandstones: A Review of the Controls on Occurrence and Behaviour During Diagenesis: Clay Mineral Cements in Sandstones, edited, pp. 109-128, Blackwell Publishing Ltd.

Naylor, D. & Shannon, P.M. (2005) The structural framework of the Irish Atlantic Margin. In Petroleum geology: N.W. Europe and Global Perspectives, Proceedings of the 6th Petroleum Geology Conference., 1009-1021.

Primmer, T.J., Cade, C.A., Evans, J., Gluyas, J.G., Hopkins, M.S., Oxtoby, N.H., Smalley, P.C., Warren, E.A. & Worden, R.H. (1997) Global patterns in sandstone diagenesis: their application to reservoir quality prediction for petroleum exploration: Reservoir quality prediction in sandstones and carbonates, AAPG Memoir, 69, 61-77.

Rateau, R., Schofield, N. & Smith, M. (2013) The potential role of igneous intrusions on hydrocarbon migration, West of Shetland: Petroleum Geoscience, 19, 259–272,

Reeckman, S.A. & Mebberson, A.J. (1984) Igneous intrusions in the north-west Canning Basin and their impact on oil exploration: Proceedings of the Canning Basin Symposium, Perth: Petroleum Exploration Society of Australia Ltd., 45–52.

Monreal, F.R., Villar, H.J., Baudino, R., Delpino, D. & Zencich, S. (2009) Modeling an atypical petroleum system: a case study of hydrocarbon generation, migration and accumulation related to igneous intrusions in the Neuquén Basin, Argentina: Marine and Petroleum Geology, 26, 590-605.

Rohrman, M. (2007) Prospectivity of volcanic basins: trap delineation and acreage de-risking: AAPG Bulletin, 91, 915–939.

Rohrman, M. (2015). Delineating the Exmouth mantle plume (NW Australia) from denudation and magmatic addition estimates: Lithosphere, 7, 589-600.

Schmiedel, T., Kjoberg, S., Planke, S., Magee, C., Galland, O., Schofield, N., Jackson, C.A.L. and Jerram, D.A., 2017. Mechanisms of overburden deformation associated with the emplacement of the Tulipan sill, mid-Norwegian margin: Interpretation 5, SK23-SK38.

Schofield, N., Holford, S., Millett, J., Brown, D., Jolley, D., Passey, S.R., Muirhead, D., Grove, C., Magee, C., Murray, J. & Hole, M. (2017) Regional magma plumbing and emplacement mechanisms of the Faroe-Shetland Sill Complex: implications for magma transport and petroleum systems within sedimentary basins: Basin Research, 29, 41-63.

Schutter, S.R. (2003) Hydrocarbon occurrence and exploration in and around igneous rocks: Geological Society, London, Special Publications, 214, 7-33.

Smallwood, J.R. & Maresh, J. (2002) The properties, morphology and distribution of igneous sills: Modelling, borehole data and 3D seismic from the Faroe-Shetland area: Geological Society, London, Special Publications, 197, 271–306.

Thomson, K. & Hutton, D. (2004) Geometry and growth of sill complexes: insights using 3D seismic from the North Rockall Trough. Bulletin of Volcanology, 66, 364-375.

Tyrrell, S., Souders, A.K., Haughton, P.D., Daly, J.S. & Shannon, P.M. (2010) Sedimentology, sandstone provenance and palaeodrainage on the eastern Rockall Basin margin: evidence from the Pb isotopic composition of detrital K-feldspar: Geological Society, London, Petroleum Geology Conference series, 7, 937-952.

Witte, J., Bonora, M., Carbone, C. & Oncken, O. (2012) Fracture evolution in oil-producing sills of the Rio Grande Valley, northern Neuquén Basin, Argentina: AAPG Bulletin, 96, 1253-1277.

Yardley, B.W.D. & Graham, J.T. (2002) The origins of salinity in metamorphic fluids: Geofluids, 2, 249-256.

Figure captions

Fig. 1. Fig. 1. (A) Location map of the Irish Rockall Basin (IRB) highlighting the distribution of igneous intrusions and extrusions (offshore central complexes, red circles; onshore central complexes and lavas, green ornament; offshore lavas, light grey ornament; seaward-dipping reflectors, dark grey ornament; hydrothermal vents, black triangles) associated with the North Atlantic Igneous Province (modified from Emeleus & Bell, 2005; Hansen, 2006). The bathymetric contours (grey lines; spacing=500 m) delineate the boundaries of the Northern Rockall Basin (NRB), Porcupine (PB), Hatton (HB), Faroe-Shetland (FSB), Møre (MB) and Vøring (VB) basins, as well as the Hatton (H) and Rockall (R) banks, and the Vøring Plateau. The Anton-Dohrn Lineament Complex (ADLC) is also labelled. (B) Bathymetry map of the Irish Rockall Basin, illustrating the location of the 3D seismic reflection survey and positions of boreholes 12/2-1 (Dooish) and 5/22-1 (Errigal). Note the proximity of the study area to the Hebridean Terrace Igneous Complex (HTIC). (C) Simplified stratigraphic column for the interval of interest depicting the key lithologies identified in boreholes 12/2-1 and 5/22-1 and our seismic-stratigraphic framework. Proven or postulated petroleum system elements are shown; So=source rock; R=reservoir rock; Se=seal rock.

Fig. 2. Arbitrary geoseismic section intersecting 12/2-1 (Dooish) and 5/22-1 (Errigal), illustrating the overall geometry of the Irish Rockall Basin, and the seismic expression, geometry and distribution of igneous sills. Note the broad, low-relief dome penetrated by 5/22-1 and its spatial relationship to the underlying igneous sill-complex, which is largely hosted in Upper Cretaceous rocks. See Fig. 1B for location. Vertical scale in two-way time in seconds (TWT s). Vertical exaggeration (VE) = *c*. x4.

Fig. 3. Interpreted seismic sections and 3D time-structure maps showing the geometry of igneous sills in the Irish Rockall Basin. See Fig. 6c and d in Magee et al. (2014) for location of sills. White lines show position of the seismic lines.

Fig. 4. Simplified stratigraphic correlation between 12/2-1 (Dooish) and 5/22-1 (Errigal) showing the principles lithologies encountered in the Upper Cretaceous to Lower Eocene succession. Lithological interpretation is based largely on cuttings and sparse sidewall cores. Pal. 1=Paleocene 1; Pal. 2=Paleocene 2. See Supplementary Material Item 1 and 5 for additional details. For location of boreholes see Figs 1B and 2.

Fig. 5. (A) Top Paleocene time-structure map (see Fig. 1C). Contour spacing = 50 m. Note the location of 5/22-1 on the crest of a broad, low-relief dome. (B) Eocene isochron (time-

thickness) map (see Fig. 1C). Note thinning of this succession across the broad, low-relief dome defined at top Paleocene level (see (A)). (C) Map depicting the geometries and stacking pattern of the 82, largely Upper Cretaceous-hosted igneous sills (see Figs 2 and 3). Note that sill stacking density is greatest immediately below the broad, low-relief dome identified at top Paleocene level (see (A)).

Fig. 6. (A) QFL (quartz-feldspar-lithics) derived from petrographic analysis of the Paleocene succession in 5/22-1 (Errigal). Location of samples is shown in Fig. 4. Raw data is shown in Supplementary Item 1. (B) Thin-section micrograph from sidewall core #38 (3587 m; Upper Paleocene). Note the dominance of volcanic rock fragments (lithics), and the subordinate quartz and feldspar. (C) Thin-section micrograph from sidewall core #18 (3916 m; Upper Paleocene). Note the dominance of detrital quartz and feldspar; rock fragments (lithics) and volcanic glass are rare. See Supplementary Material Item 1 for additional petrographic data.

Fig. 7. Plot showing fluid inclusion microthermometry data from 5/22-1 (Errigal). Note the overall low homogenisation temperatures (<90º) for all samples. See text for full discussion. See Supplementary Material Item 3 for additional fluid inclusion-derived, microthermometric data.

Fig. 8. (A) Table showing vitrinite reflectance (VR) and paleotemperature analysis interpretation of VR data from 5/22-1 (Errigal). 'Measured VR' values are mean random reflectance values for each sample. Estimates of maximum paleotemperature were determined using assumed heating rates 1ºC/Ma and a cooling rates of 10ºC/Ma. (B) Plot of VR vs. depth for 5/22-1 (Errigal). See text for full discussion. See Supplementary Material Item 3 for additional details on paleothermal modelling parameters.

Fig. 9. (A) Table showing Apatite Fission Track Analysis (AFTA) data for 5/22-1 (Errigal). Note that present temperature estimates based on an assumed mean seabed temperature of 5ºC and a present-day thermal gradient of 26.5ºC/km. Thermal history interpretation of AFTA data is based on an assumed heating rate of 1ºC/Ma and a cooling rate of 10ºC/Ma. Quoted ranges for paleotemperature and onset of cooling correspond to ±95% confidence limits. Values represents paleo-thermal effects that are allowed but not definitely required by available data. See Supplementary Item 3 for additional details on paleothermal modelling parameters and uncertainties. (B) AFTA data (left) and present temperature (right) plotted against sample depth (and stratigraphic age). The dashed black line on the left-hand panel indicates the stratigraphic age of the penetrated succession. Note that in all cases, fission track ages are significantly higher than the respective stratigraphic ages, suggesting: (i) these apatites contains a large

proportion of fission tracks formed prior to deposition of the host sediments; and (ii) post-depositional heating effects were modest. (C) Preferred thermal history interpretation of AFTA and VR data from 5/22-1 (Errigal).

Supplementary Item 1. Well IRE 5/22-1 “Errigal Deepwater Exploration” Final Well Report. Volume 1: Geological and Petrophysical Evaluation. Republic of Ireland Continental Shelf Oil Well Records. Prepared by Toby Lenehan. Published in 2001. Report provided by the Petroleum Affairs Division (PAD). Curated by IHS Energy. Available for download from: https://www.dccae.gov.ie/en-ie/natural-resources/topics/Oil-Gas-Exploration-Production/data/Pages/Data.aspx.

Supplementary Item 2. Wellsite litholog for ERRIGAL IRE 5/22-1. Wellsite geologists: James Hollands and Alastair Flood. Provided by the Petroleum Affairs Division (PAD). Available for download from: https://www.dccae.gov.ie/en-ie/natural-resources/topics/Oil-Gas-Exploration-Production/data/Pages/Data.aspx.

Supplementary Item 3. Evidence for the conditions of cementation and petroleum emplacement from fluid inclusions, Eastern Rockall Basin, Eire. Republic of Ireland Continental Shelf Oil Well Records. Prepared by FIA. Report provided by the Petroleum Affairs Division (PAD). Curated by IHS Energy. Available for download from: https://www.dccae.gov.ie/en-ie/natural-resources/topics/Oil-Gas-Exploration-Production/data/Pages/Data.aspx.

Supplementary Item 4. Thermal history reconstruction in Errigal deepwater exploration well 5/22-1, using AFTA and vitrinite reflectance. Republic of Ireland Continental Shelf Oil Well Records. Published in 2001. Geotrack report #807. Prepared by P.F.Green (Geotrack). Report provided by the Petroleum Affairs Division (PAD). Curated by IHS Energy. Available for download from: https://www.dccae.gov.ie/en-ie/natural-resources/topics/Oil-Gas-Exploration-Production/data/Pages/Data.aspx.

Supplementary Item 5. IRE 12/2-1 Dooish composite log. Wellsite geologists: Peter Geerlings and Nick O’Neill. Log compiled by Peter Geerlings and Toby Lenehan. Report provided by the Petroleum Affairs Division (PAD). Available for download from: https://www.dccae.gov.ie/en-ie/natural-resources/topics/Oil-Gas-Exploration-Production/data/Pages/Data.aspx.

Supplementary Item 6. Geochemical report on well 5/22-1. Republic of Ireland Continental Shelf Oil Well Records.Published in 2001. Authored by Peter B. Hall (GeoLab Nor A/S). Report provided by the Petroleum Affairs Division (PAD). Curated by IHS Energy. Available for download from: https://www.dccae.gov.ie/en-ie/natural-resources/topics/Oil-Gas-Exploration-Production/data/Pages/Data.aspx.

Fig. 1

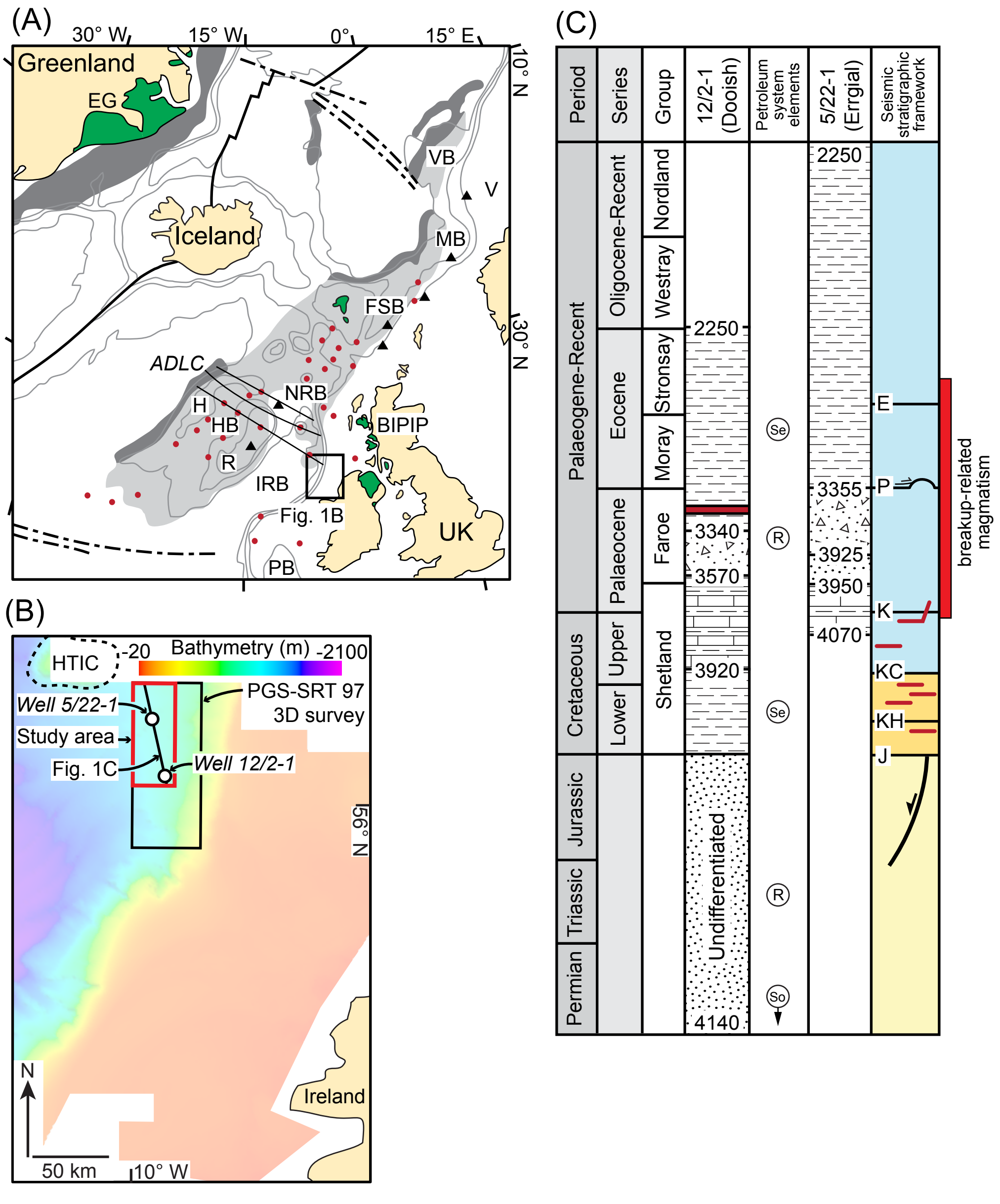
(A)
30° W
15° W
0°
15° E
Greenland
EG
Iceland
VB
V
MB
FSB
ADLC
NRB
H
HB
R
BIPIP
IRB
Fig. 1B
UK
PB
10° N
30° N
(B)
HTIC
Bathymetry (m)
-20
-2100
Well 5/22-1
PGS-SRT 97
3D survey
Study area
Fig. 1C
Well 12/2-1
56° N
N
50 km
10° W
Ireland
(C)
Period
Series
Group
12/2-1 (Dooish)
Petroleum system elements
5/22-1 (Errgial)
Seismic stratigraphic framework
Palaeogene-Recent
Oligocene-Recent
Eocene
Palaeocene
Nordland
Westray
Stronsay
Moray
Faroe
Cretaceous
Upper
Lower
Shetland
Jurassic
Triassic
Permian
Undifferentiated
2250
3340
3570
3920
4140
3355
3925
3950
4070
Se
R
So
E
P
K
KC
KH
J
breakup-related magmatism

Fig. 2

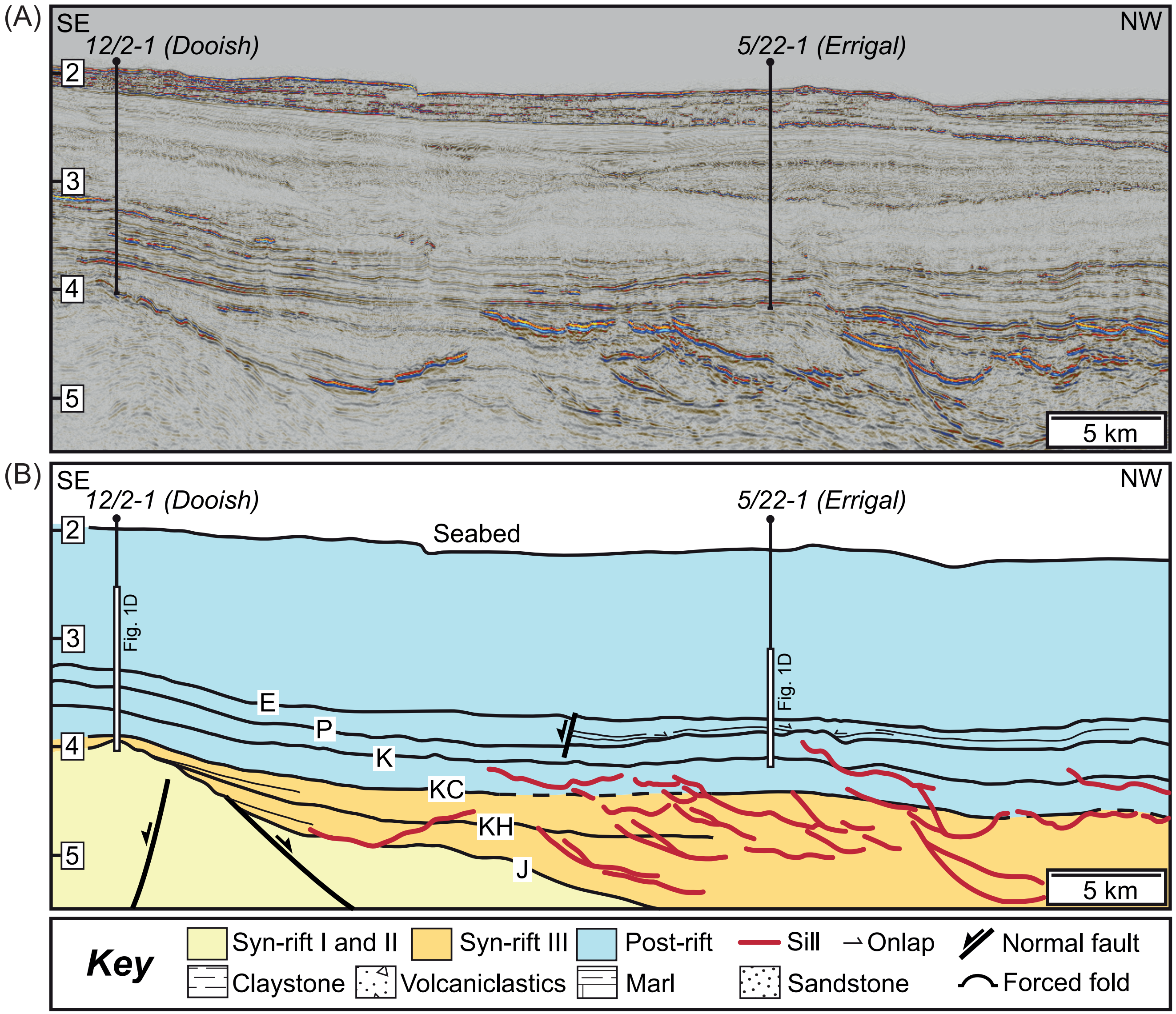

(A)
SE
NW
12/2-1 (Dooish)
5/22-1 (Errigal)
2
3
4
5
5 km
(B)
SE
NW
12/2-1 (Dooish)
5/22-1 (Errigal)
Seabed
Fig. 1D
Fig. 1D
E
P
K
KC
KH
J
2
3
4
5
5 km
Key
Syn-rift I and II
Syn-rift III
Post-rift
Sill
Onlap
Normal fault
Claystone
Volcaniclastics
Marl
Sandstone
Forced fold

Fig. 3

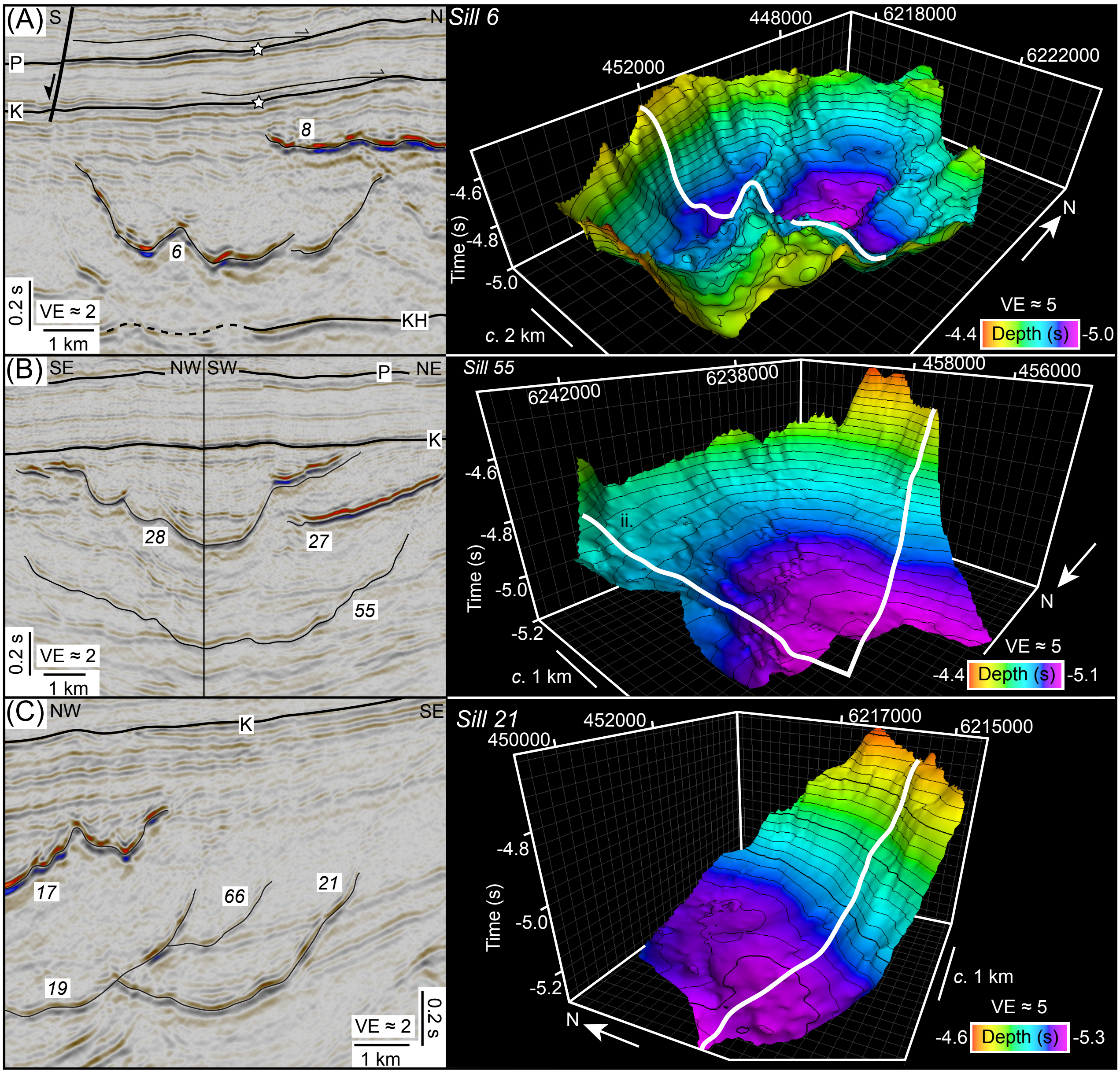

(A)
S
N
P
K
8
6
0.2 s
VE ≈ 2
1 km
KH
Sill 6
448000
6218000
452000
6222000
-4.6
-4.8
-5.0
Time (s)
N
c. 2 km
VE ≈ 5
-4.4
Depth (s)
-5.0
(B)
SE
NW
SW
P
NE
K
28
27
55
0.2 s
VE ≈ 2
1 km
Sill 55
6242000
6238000
458000
456000
-4.6
-4.8
-5.0
-5.2
Time (s)
ii.
N
c. 1 km
VE ≈ 5
-4.4
Depth (s)
-5.1
(C)
NW
K
SE
17
66
21
19
VE ≈ 2
0.2 s
1 km
Sill 21
452000
450000
6217000
6215000
-4.8
-5.0
-5.2
Time (s)
N
c. 1 km
VE ≈ 5
-4.6
Depth (s)
-5.3

Fig. 4

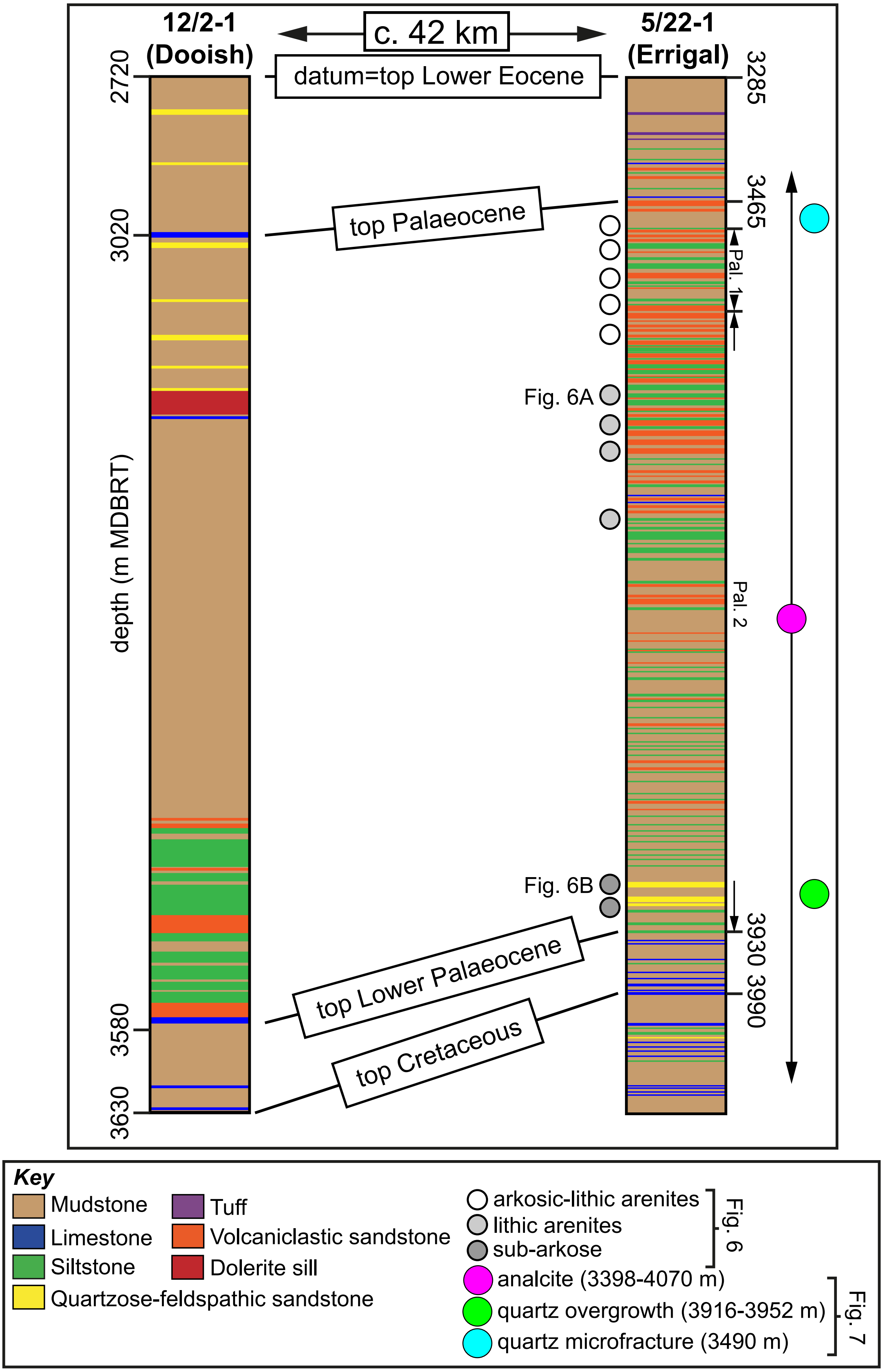

12/2-1
(Dooish)
c. 42 km
5/22-1
(Errigal)
datum=top Lower Eocene
2720
3020
3580
3630
depth (m MDBRT)
3285
3465
3930
3990
top Palaeocene
Pal. 1
Pal. 2
Fig. 6A
Fig. 6B
top Lower Palaeocene
top Cretaceous
Key
Mudstone
Limestone
Siltstone
Quartzose-feldspathic sandstone
Tuff
Volcaniclastic sandstone
Dolerite sill
arkosic-lithic arenites
lithic arenites
sub-arkose
Fig. 6
analcite (3398-4070 m)
quartz overgrowth (3916-3952 m)
quartz microfracture (3490 m)
Fig. 7

Fig. 5

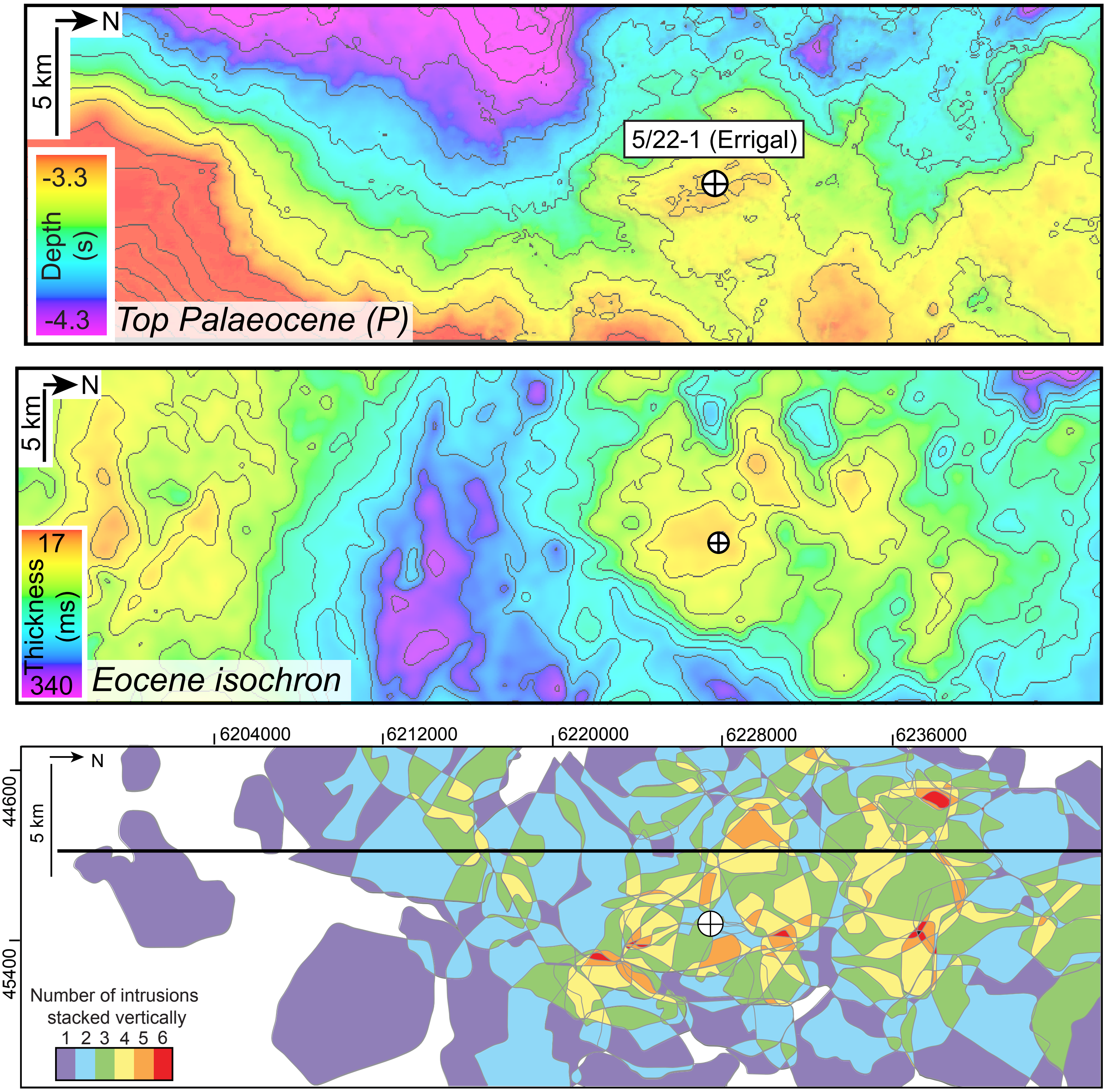
N
5 km
5/22-1 (Errigal)
-3.3
Depth (s)
-4.3
Top Palaeocene (P)
N
5 km
17
Thickness (ms)
340
Eocene isochron
6204000
6212000
6220000
6228000
6236000
44600
45400
N
5 km
Number of intrusions stacked vertically
1 2 3 4 5 6

Fig. 6

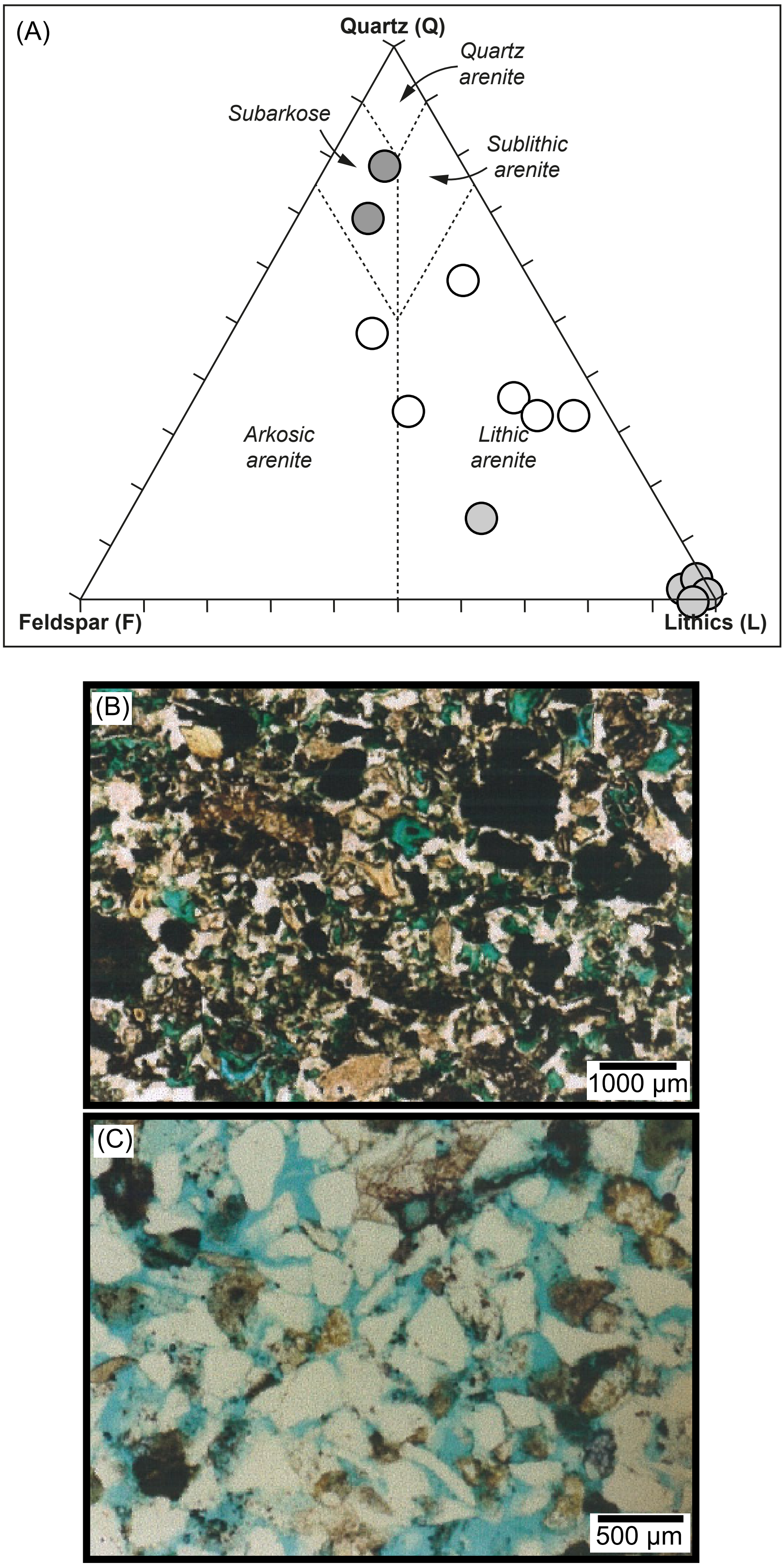

(A)
Quartz (Q)
Quartz arenite
Subarkose
Sublithic arenite
Arkosic arenite
Lithic arenite
Feldspar (F)
Lithics (L)
(B)
1000 μm
(C)
500 μm

Fig. 7

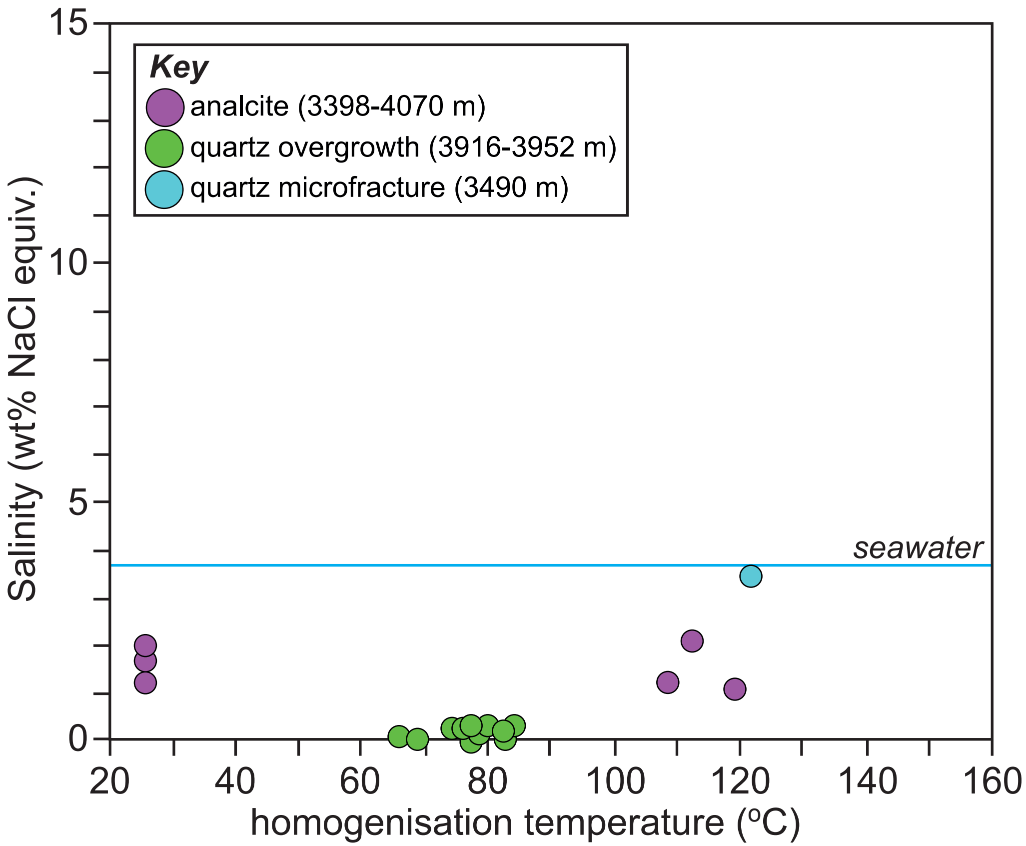

15
10
5
0
20
40
60
80
100
120
140
160
Salinity (wt% NaCl equiv.)
homogenisation temperature (ºC)
Key
analcite (3398-4070 m)
quartz overgrowth (3916-3952 m)
quartz microfracture (3490 m)
seawater

Fig. 8

(A)

Average Depth (m)	Present temperature (°C)	Stratigraphic age (Ma)	Measured VR (%)	Number of readings	Maximum paleotemperature (°C)
2589	29	35-16	0.42	3	70
2643	31	35-16	0.27	7	<50
2697	32	35-16	0.36	4	59
2751	34	35-16	0.33	8	50
2823	36	42-35	0.33	20	50
2871	37	42-35	0.33	20	50
2931	38	42-35	0.35	20	56
2991	40	42-35	0.33	20	50
3051	42	42-35	0.33	20	50
3111	43	42-35	0.38	20	63
3171	45	42-35	0.42	20	70
3231	46	42-35	0.41	20	69
3291	48	42-35	0.44	20	74
3339	49	42-35	0.48	20	80
3387	50	42-35	0.47	1	79
3450	52	56-42	0.45	13	76
3510	54	56-42	0.46	14	78
3570	55	56-42	0.47	1	79
3630	57	60-56	0.39	3	65
3690	59	60-56	0.42	4	70
3750	60	60-56	0.45	13	76
3810	62	60-56	0.45	17	76
3870	63	60-56	0.44	4	74
3930	65	65-60	0.44	11	74
3990	66	65-60	0.47	3	79
4050	68	74-65	0.47	2	79

(B)

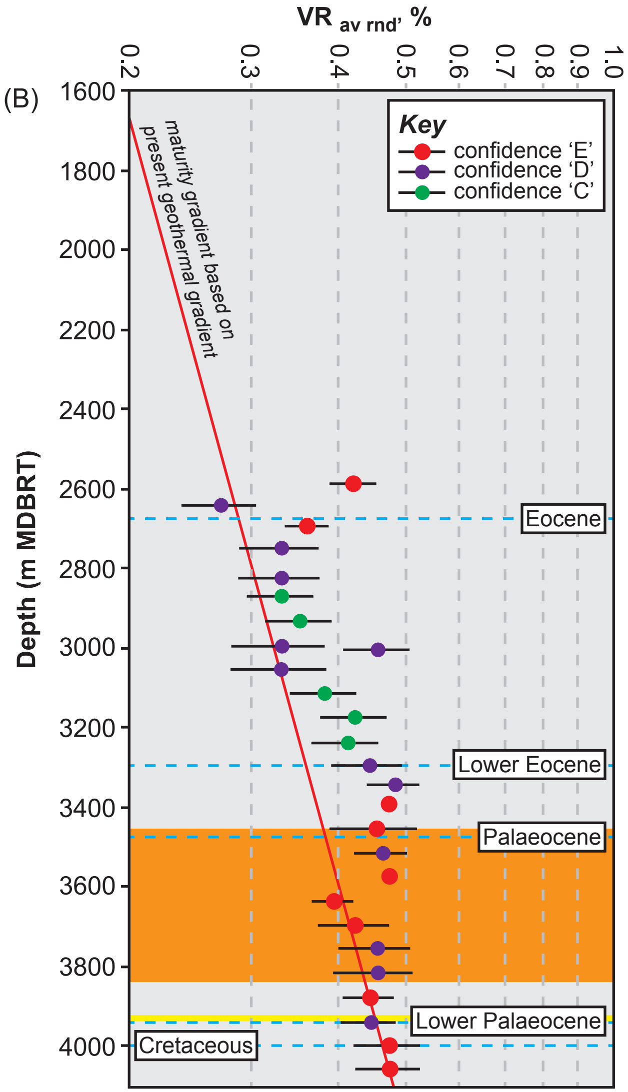

N.B. error bars=one standard deviation

Fig. 9

(A)

Sample number	Mean depth (mkb)	Stratigraphic age (Ma)	Present temperature (°C)	Maximum paleotemperature (°C)	Onset of cooling (Ma)
GC807-1	2671	42-16	31	<100	post-depositional
GC807-2	2925	42-35	38	<110	post-depositional
GC807-3	3175	42-35	45	60-90	post-depositional
GC807-4	3438	60-35	52	80-100	post-depositional
GC807-5	3688	60-56	58	75-90	40-0
GC807-6	3936	74-56	65	75-100	post-depositional
GC807-7	3936	74-56	65	80-100	>10
				Overlap:	40-10